Residual Stresses after Orthogonal Machining of AISI 304: Numerical Calculation of the Thermal Component and Comparison with Experimental Results

CHRISTOPH WIESNER

Residual stresses due to the thermal influence of orthogonal machining have been calculated with a finite element model using stationary workpiece temperatures during cutting calculated with the finite difference method. Calculated results are compared with experimental data obtained with the X-ray diffraction method. In this way, the thermal and mechanical/frictional influences of the machining operation on the workpiece residual stress state can be separated. The influence of cutting speed and cutting depth on machining residual stresses is discussed. It is shown that the thermal as well as the mechanical impact of the orthogonal cutting process causes tensile residual stresses. The mechanical impact of the machining operation causing tensile residual stresses is due to (a) compressive plastic deformation in the surface layer ahead of the advancing tool and (b) greater elastic relaxation upon unloading with respect to the underlying material of a thin, strongly work-hardened surface layer.

I. INTRODUCTION

MANY properties are dependent on the geometrical, mechanical, and structural surface and near-surface conditions of a component. The surface and the superficial surface layer can be characterized by their topographies, *e.g.*, Reference 1, their microstructure/hardness profiles, *e.g.*, Reference 2 and their residual stresses. These characteristics are strongly influenced by machining operations and their parameters.[3] This article concentrates on the residual stress state caused by orthogonal cutting; the geometry and the forces and angles during orthogonal planing are shown in Figure 1. Residual stresses strongly influence many material properties and therefore have been of interest over the last 10 years.[4–7] The near-surface residual stresses are produced during machining primarily by mechanical and thermal impacts:

(1) The mechanical impact is generally said to cause compressive residual stresses. This is true for near-surface plastic elongation which is constrained by the undeformed bulk material and causes compressive residual stresses. However, there are modifications of the surface layer caused by the mechanical impact of the tool which produce tensile residual stresses. (a) Strong work hardening and a considerable increase in microstructural defect density close to the surface during machining causes greater elastic relaxation upon unloading of a thin surface layer compared with the underlying workpiece. This relaxation is constrained by the bulk material, and tensile residual stresses are formed.[8] (b) Thermomechanical elastoplastic stress analyses of orthogonal machining using the shear plane as a boundary condition[9] have shown that there are two plastic deformation zones in the surface layer during cutting. A large compressive plastic deformation zone is formed ahead of the advancing tool and a tensile plastic deformation zone behind it. This is illustrated in Figure 2 from Reference 9. The material in the surface layer is thus twice plastically deformed (with changing signs) during machining. Cutting conditions used for the calculations in Reference 9 cause greater effective plastic conpression ahead of the tool than tensile plastic deformation behind the tool, as can be seen in Figure 2. Therefore, a wake of plastically compressed material is left in the surface layer. The plastic deformations are constrained by the undeformed bulk of the workpiece which produces tensile residual stresses.

(2) Strong thermal gradients in the workpiece during cutting produce thermal expansion of the near-surface region which is constrained by the cool bulk regions. This can lead to compressive plastic deformations of the superficial layer facilitated by the low yield strength at high temperature and results in tensile residual stresses. In addition, microstructural changes, such as dynamic recovery or recrystallization, phase transformation, and diffusion processes, are thermally activated and can take place in the heated surface layer if the temperatures reached are sufficient. These processes can weaken the material or provoke volume changes which also influence the residual stress state.

A complete calculation of residual stresses due to machining is difficult, since a combination of mechanical, thermal, and tribological (frictional) loadings as well as possible phase transformation effects have to be taken into account. Therefore, to the author's knowledge, there have been few attempts to calculate the residual stresses produced due to machining.[10–13] Since the calculation of residual stresses involves elastic-plastic material behavior and temperature-dependent material properties, numerical methods have been employed in these articles.

In this work, the residual stresses after planing of an AISI-304 austenitic steel are measured with the X-ray method, and the influence of cutting speed and cutting depth is investigated. The residual stresses caused by the thermal expansion due to superficial heating of the workpiece are calculated with a finite element model using

CHRISTOPH WIESNER, formerly Research Assistant with the Laboratoire de Métallurgie Mécanique, Ecole Polytechnique Fédérale de Lausanne, MX-D Ecublens, 1015 Lausanne, Switzerland, is Senior Research Engineer with TWI (The Welding Institute), Engineering Department, Abington Hall, Abington, Cambridge CB1 6AL, England.

Manuscript submitted April 5, 1991.

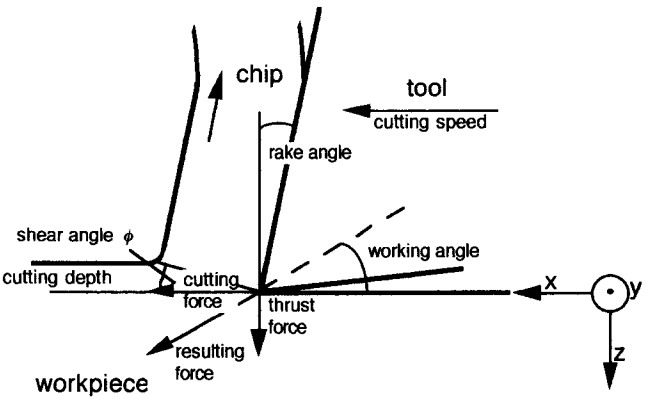

Fig. 1—Two-dimensional representation of the orthogonal planing process illustrating the forces and angles appearing in Table I.

workpiece temperature distributions calculated with a finite difference method.[14] The calculated thermal residual stresses do not represent the real situation in the machined workpiece. However, knowledge of them allows us to separate the mechanical and thermal influences of the machining operation on the residual stress state: the difference between the measured residual stresses (caused by the combination of a mechanical and a thermal impact) and the calculated residual stresses (thermal loading only) can be identified with the component of the residual stress state which is caused by the mechanical impact of the tool on the workpiece during machining. In that way, thermal and mechanical residual stresses due to the orthogonal machining operation can be separated and the different influences can be quantitatively discussed.

The influence of phase transformations on the residual stress state during orthogonal cutting is assumed to be negligible in this work, since the determined maximum workpiece temperatures of ≈450 °C[14] are too low to cause phase transformation in this material during the very short heating period.

II. EXPERIMENTAL

For X-ray measurements of residual stresses,[4,5,15] an Ω-diffractometer equipped with a scintillation detector and a polycrystalline monochromator was employed. The ψ-tilt and 2θ rotation as well as data acquisition and evaluation were controlled by a microcomputer. The background noise was subtracted from the intensities across a peak using a linear fit of the first and the last 5 pct of

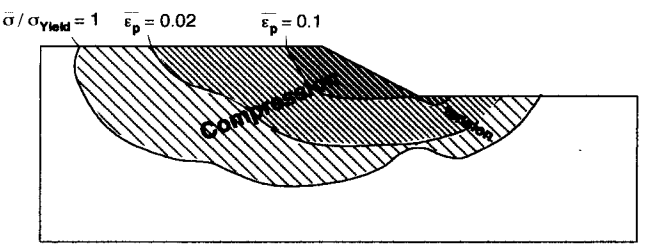

Fig. 2—Primary plastic deformation zone during orthogonal machining of a low carbon-free cutting steel (cutting speed = 2.6 m/s, cutting depth = 0.274 mm, and rake angle = 20 deg).[9]

the measured data. The net intensities were corrected for absorption and for the Lorentz polarization factor. The 2θ position was calculated as the center of gravity of the peak. The dispersion of the X-rays was limited to 1 deg. Measurements were made using Cu K_α-radiation which penetrates only ≈1.4 μm into the studied material at $\sin^2 \psi = 0.3$. Eleven ψ-tilts were examined at an azimuth angle ϕ of 0 deg. Measured lattice strain distributions, *i.e.*, the plot of $(D_{\phi\psi} - D_0)/D_0$ *vs* $\sin^2 \psi$, were linear.[16] The terms $D_{\phi\psi}$ and D_0 are the measured and the unstressed {331} interplanar spacings, respectively, and ψ is the angle between the normal to the diffracting plane and the normal to the specimen's surface. ψ-splitting for $\psi \lesssim 0$ or curved lattice strain distributions could not be distinguished within the range of data scatter if measurements were repeated at different sample positions. Therefore, a biaxial stress state prevails in the sampled volume of material ($\sigma_{13}, \sigma_{23}, \sigma_{33} = 0$). X-ray elastic constants for the austenitic phase used for the stress calculation from the measured lattice strains of the {331} planes for AISI-304 were taken from Reference 4. Pseudo-macro residual stresses which arise due to stresses carried by phase or grain boundaries[17] can contribute to the residual stresses measured by X-rays.[18] It is assumed in this work that such stresses are small and do not affect the trends shown in this work.

Depth-profiles of residual stresses were obtained by electrochemical removal of material layers. Specimens were machined orthogonally on a planing machine, and different cutting speeds and cutting depths were employed. Previously, the specimens were heat-treated 1 hour at 1100 °C and slowly cooled in the furnace to avoid the formation of residual stresses due to rapid cooling. A constant rake angle of 0 deg and hard metal tool inserts were employed. Cutting forces were measured using a dynamometer. The cutting conditions and the resulting forces and angles are listed in Table I.

The results of the residual stress measurement are shown in Figure 3. Figure 3(a) shows the influence of the cutting speed on the residual stress distribution parallel to the cutting direction σ_x (*cf.* Figure 1). The variation due to the cutting speed is elucidated by the arrows in Figure 3(a). High tensile residual stresses (≈700 MPa) which decrease quickly in the depth direction of the specimen are present at the surface. In 400- to 600-μm depth, a compressive residual stress region is reached. There is a certain scatter of the data which is due to the fact that measurements have been made at different sample positions; it is shown in References 19 and 20 that residual stresses vary markedly if measured at different specimen locations. The influence of increasing cutting speed on the mean residual stress values (indicated by the lines in Figure 3(a)) is clear. At low cutting speed, the tensile residual stresses reach deeper into the workpiece, and thus, the compressive region commences at greater depths. Similar results have been obtained after planting C1018 steel.[21,22]

The influence of cutting depth on the residual stresses after planing is shown in Figure 3(b). The overall shape of the residual stress-depth curves remains similar to Figure 3(a). Increasing cutting depth leads to an augmentation of the stresses in the tensile region, and in order to balance this, the compressive stresses are also

Table I. Cutting Conditions and Measured Cutting Forces and Angles of the Investigated Specimens*

Cutting Condition	Cutting Depth t_1 (mm)	Cutting Speed v (m/s)	Shear Angle ϕ (deg)	Cutting Force F_C (N)	Thrust Force F_T (N)	Stress Ratio μ	Working Angle β (deg)
A	0.08	0.15	4	1024	844	1.08	39
B	0.07	0.58	10	601	470	0.91	38
C	0.08	1.05	16	660	510	0.73	38
D	0.16	1.05	18	1120	725	0.82	33
E	0.20	1.05	20	1349	782	0.84	30

*Orthogonal planing, rake angle = 0 deg, specimen width = 3.0 mm. The shear angle was determined from $\tan \phi = t_1 \cos \gamma/(t_2 - t_1 \sin \gamma)$, where t_2, t_1, and γ are the average chip thickness, the cutting depth, and the rake angle, respectively. $\mu = \tau_S/\sigma_S = (1 - F_C/F_T \tan \phi)/(\tan \phi + F_T/F_C)$ is the ratio of tangential to normal stress in the shear plane.

greater. A rise of tensile residual surface stresses with increasing cutting depth in planing a 0.45 pct C steel has also been measured in Reference 12. Increasing the feed in turning a 0.45 pct C steel which can be compared to an increase of the cutting depth in planing also leads to changes of the residual stresses comparable to Figure 3(b).[23]

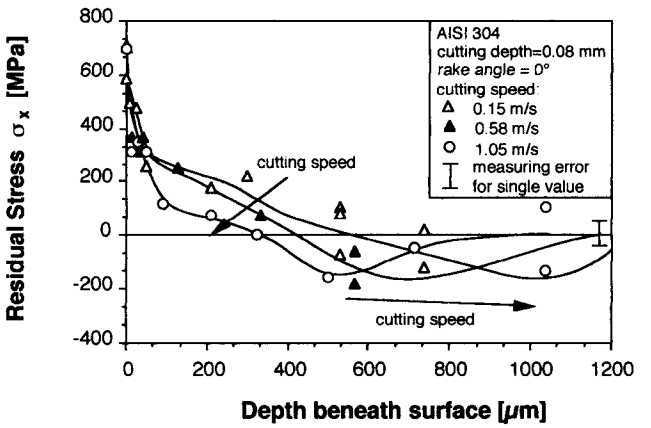

(*a*)

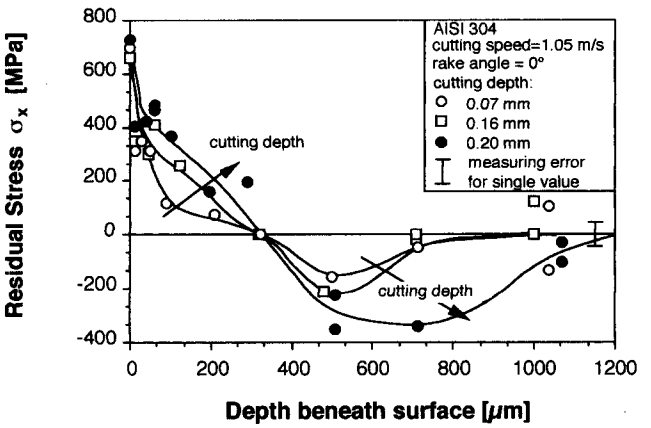

(*b*)

Fig. 3—(*a*) Measured influence of cutting speed on residual stress distributions after planing of AISI 304 using the X-ray diffraction method. (*b*) Experimental residual stress profiles after planing of AISI 304 at different cutting depths. The variation of the residual stress profiles with cutting speed or cutting depth is elucidated by the arrows.

III. CALCULATION

The thermal impact on the near-surface region, *i.e.*, the workpiece temperatures during planing, was calculated numerically using a finite difference method and also measured by infrared pyrometry. Details of the methods and results have been published elsewhere.[14] The principle of the calculation is as follows. The cutting energy is determined using cutting force measurements. The part of the cutting energy entering the workpiece is taken from available experimental and numerical data; this part includes the heat which is created in the workpiece by plastic deformation of the surface layer, and the heat created by friction between the tool clearance face and the workpiece surface which enters the workpiece. A triangular distribution of the power with its maximum at the cutting edge is assumed. The governing equation for the steady-state temperature field produced by a moving heat source is solved using a finite difference model with temperature-dependent thermal properties. The boundary temperatures of the model are given by an analytical solution of the heat equation for a moving line heat source in order to consider just the heat-affected region. Further details of the calculation and experimental validation can be found in References 14, 24, and 25. An example of a calculated temperature field and the corresponding temperature-time-depth curves during planing is shown in Figures 4(a) and (b) for cutting condition A in Table I. The tool edge in Figure 4(a) corresponds to time = 0 in Figure 4(b). For each cutting condition, the corresponding workpiece field was calculated. The results for cutting conditions C and E are shown in Figures 5(a) and (b).

In order to calculate the thermally induced residual stresses due to cutting a one-row model of the workpiece, Figure 6(b) is devised in discrete plane strain isoparametric elements using a commercial finite element code.[26] The plane strain assumption ($\varepsilon_y = 0$) is acceptable as long as the ratio of cutting depth to width (in y-direction) of the specimen remains sufficiently small (the maximum ratio used in machining in this work was 0.05). The boundary conditions are as follows: lower edge: $u_z = 0$; and right- and left-hand edges: $u_x = 0$, where u_i are the displacements. Thus, the model is fully constraint in the x-direction. Preliminary calculations using a two-dimensional (2-D) model of the whole workpiece depicted in Figure 6(a) showed that thermally caused displacements, u_x, in the center of the model are very

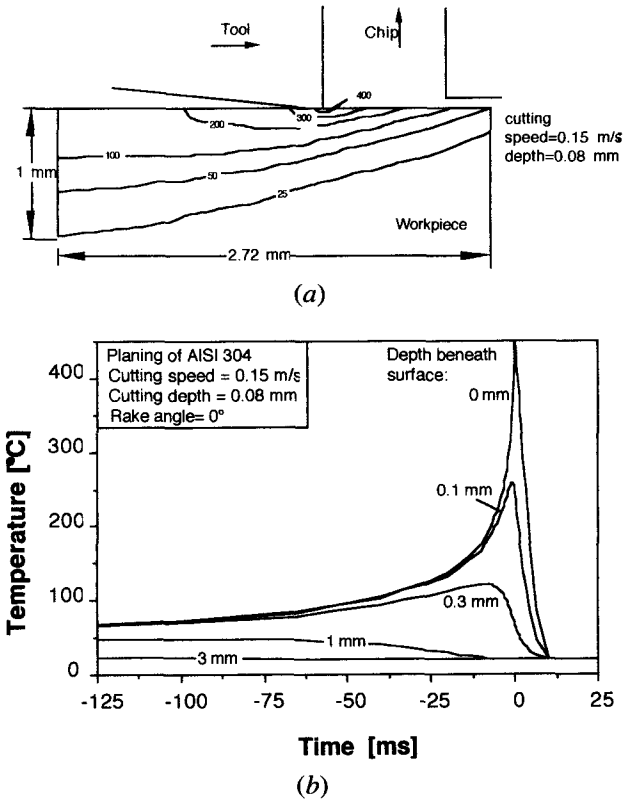

Fig. 4—Calculated workpiece temperatures for cutting condition A in Table I: (*a*) workpiece temperature field, isotherms in deg C; and (*b*) corresponding temperature-time-depth curves.

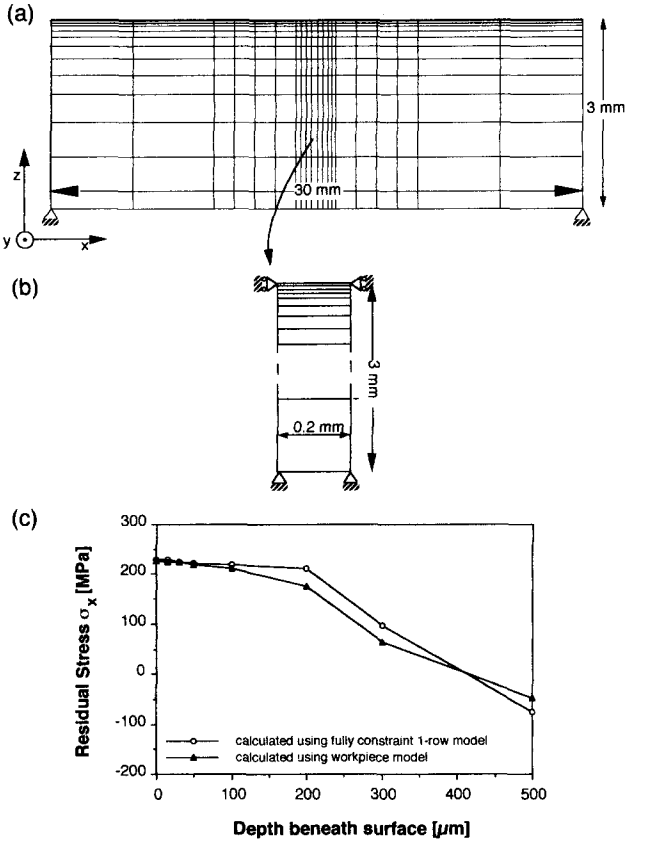

Fig. 6—(*a*) 2-D finite element model of the workpiece used to calculate thermally induced residual stresses. (*b*) One-row finite element mesh of the workpiece. (*c*) Comparison of the calculated residual stress distribution using meshes (a) and (b), respectively.

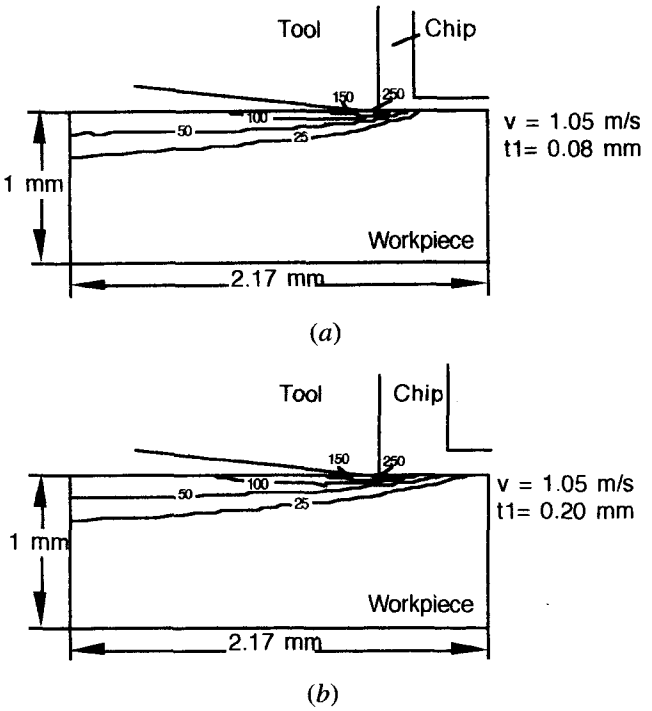

Fig. 5—Influence of cutting depth on calculated workpiece temperature fields (cutting conditions (*a*) C and (*b*) E from Table I): isotherms are in deg C; v is the cutting speed; and t_1 is the cutting depth.

small (maximum $\approx 10^{-7}$ mm). Therefore, almost equal residual stress distributions are obtained using the fully constraint one-row model or the 2-D model of the workpiece (Figure 6(c)). To save calculation time, the one-row model has been used throughout this work. This one-row model contains 12 isoparametric plane strain four-node elements. According to its position with respect to the surface, each node of the model is assigned a temperature-time curve for the given depth calculated previously (*e.g.*, Figure 4(b)). The advance of the tool is modeled by shifting these curves for each row in the model by $\Delta x/v$, where Δx is the mesh width in the direction of the tool movement and v is the cutting speed. The temperature rise ΔT in the superficial layer of the workpiece produces thermal strains ε_{th} according to the thermal expansion coefficient $\alpha(T)$ of the investigated material; *i.e.*,

$$\varepsilon_{th} = \alpha(T)\,\Delta T \qquad [1]$$

These deformations are constrained by the unheated rest of the workpiece and produce compressive yield of the surface region facilitated by the lower yield strength at high temperatures. Constrained thermal contraction during cooling of the plastically deformed surface region on the bulk specimen provokes tensile residual stresses.

Calculations have been carried out using temperature-dependent Young's modulus, Poisson's ratio, thermal expansion coefficient, and stress-strain relations for this material. Stress-strain curves of the investigated material

were measured in tensile tests at room temperature. Their temperature dependence was extrapolated using experimental data for this material.[27] From the same reference, temperature-dependent values for Young's modulus, Poisson's ratio, and linear thermal expansion coefficient were taken. The material properties employed in this work are represented in Table II. Plastic flow is modeled in the used FEM code using the von Mises flow criterion and a rate-independent incremental plasticity model with isotropic hardening.[26]

The results of the thermal residual stress calculations are shown in Figure 7. As in Figure 1, only the stress components parallel to the cutting direction σ_x are shown. The residual stress distributions perpendicular to the cutting direction σ_y are almost identical to the parallel one in Figure 7 and have, therefore, been omitted in the interest of clarity. The calculated values for σ_z and σ_{xz} are very small (maximum ≈7 MPa) and have been omitted from the figures. Figure 7(a) shows the influence of the cutting speed on the thermal residual stresses. It demonstrates how a reduction of the cutting speed leads to an extension of the tensile residual stress domain. The surface values of the residual stresses decrease with growing cutting speed (268 MPa at 0.15 m/s and 236 MPa at 1.05 m/s). The compressive residual stress region is shifted to higher compressive values and to greater depth in order to balance the larger tensile region at lower speeds. Figure 7(b) shows that the influence of the cutting depth on the calculated thermal residual stresses is small.

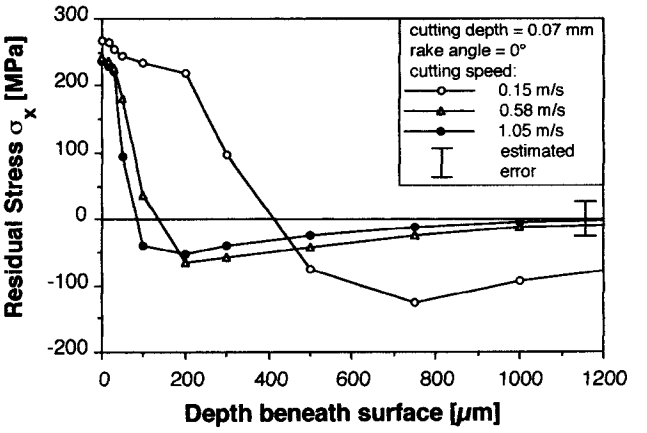

(a)

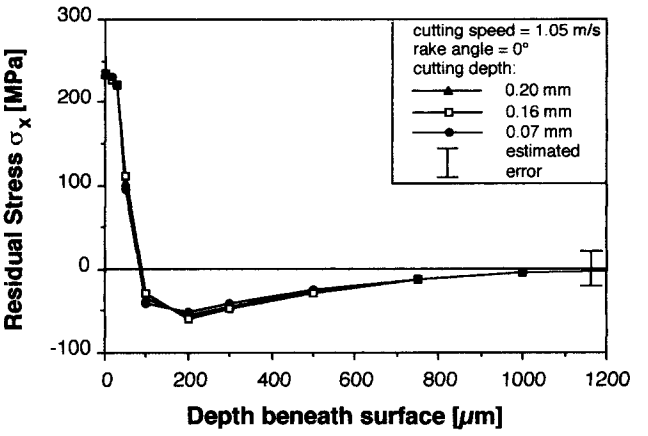

(b)

Fig. 7—Calculated thermal residual stresses due to planing of AISI 304: (*a*) influence of cutting speed; and (*b*) influence of cutting depth.

IV. DISCUSSION

A. *Influence of Cutting Speed*

It can be seen from Figures 4(a) and 5(a) that the maximum workpiece temperatures and the depth to which the workpiece is heated rise with decreasing cutting speed during planing. It is shown in Reference 14 that due to an increase in chip speed and the small thermal diffusivity of this material, a greater fraction of the cutting energy (which increases with cutting speed) is carried away with the chip. Hence, the energy entering the workpiece grows only slightly with increasing cutting speed. This small rise in cutting energy is not sufficient to balance the convection effect which becomes more important at high cutting speeds. Therefore, workpiece temperatures and the depth of the heated zone reduce with increasing cutting speed during planing of this material (Figure 4(a) (T_{max} = 448) in contrast to Figure 5(a) (T_{max} = 310 °C)). Thus, the tensile stress domain close to the surface is largest and the surface residual stress is highest at the lowest cutting speed employed (Figure 7(a)).

The experimental results (Figure 3(a)) show a similar variation of residual stress with changing cutting speed. Thus, the thermal influence on residual stresses during machining of this material is quite important. A comparison between measured and calculated values, however, reveals considerable differences of the surface

Table II. Temperature-Dependent Material Properties of the Investigated AISI 304 Austenitic Steel*

E (GPa)	ν	$R_{p=0.02}$ (MPa)	R_m (MPa)	ε_{pl} (R_m)	$\alpha \cdot 10^{-6}$ (1/°C)	T (°C)
196.0	0.262	220	1015	0.48	10.7	20
194.0	0.266	209	951	0.49	13.6	50
190.5	0.273	197	891	0.50	17.4	100
182.5	0.288	170	816	0.53	23.4	200
168.0	0.319	120	748	0.58	32.4	400
150.4	0.295	90	700	0.70	41.7	600

*E is Young's Modulus, ν Poisson's ratio, $R_{p=0.02}$ the yield strength at 0.2 pct plastic deformation (ε_{pl}), R_m the maximum tensile strength, α the linear thermal expansion coefficient, and T the temperature (true stress and strain values). Data for E, ν, and α as well as the temperature dependence for $R_{p=0.02}$, R_m, and ε_{pl} (R_m) were taken from Ref. 27.

residual stresses (calculated thermal residual surface stress ≈250 MPa; and measured surface value ≈700 MPa). The obvious conclusion is that the mechanical and frictional impacts of the tool lead to surface layer modifications which increase the tensile residual stresses.

Near-surface tensile residual stresses caused by the mechanical impact of the tool during machining can be attributed to (a) the compressive plastic deformation zone ahead of the advancing tool (Figure 2) and (b) the work hardening of and the considerable increase in defect density[2,28] in the surface layer causing greater elastic relaxation upon unloading compared with the underlying bulk material.[8]

As pointed out in References 9 and 29, the surface layer material yields twice during cutting. If the compressive deformations are higher than the tensile deformations, as in the case of Figure 2, a wake of plastically compressed material is left behind in the surface layer. These compressive deformations are constrained by the bulk workpiece and tensile residual stresses are produced.

Factors influencing the size of the compressive zone and the magnitude of the compressive strains are analyzed in Reference 30. The authors show that the extent of compressive deformation in the surface layer (and thus the tensile residual stress) increases with decreasing shear angle ϕ, decreasing ratio μ of tangential to normal stress in the primary deformation zone (the shear plane region), rising workpiece temperatures, and increasing yield strength.

In References 12 and 13, it has been proposed that a decreasing working angle (that is the angle between resultant cutting force and the cutting direction, as indicated in Figure 1) enhances the mechanical influence of the cutting process which causes tensile residual stresses.

It can be seen from Table I that increasing the cutting speed leads to an increase in the shear angle and a decrease in the stress ratio μ and the workpiece temperatures (Figures 4 and 5). The working angle remains relatively constant. Thus, there are two factors (shear angle ϕ and temperature) which decrease the compressive deformation (and the formation of tensile residual stresses) in the surface layer and one factor (stress ratio μ) which enhances tensile residual stresses when increasing the cutting speed. Since the net effect of the different factors determines the real residual stress state (Figure 3), it is the effect of decreasing temperatures and increasing shear angle which dominates the change of residual stresses when the cutting speed is increased. A comparison of the experimental and numerical results shows that the influence of the mechanical impact of the tool causing tensile residual stresses becomes more important at higher cutting speeds as the difference between calculated purely thermal and measured residual stresses becomes greater. It can be concluded that the influence of the (increasing) shear angle becomes more important at high cutting speeds for this material and this machining operation.

In addition, the relaxation effect as explained in (b) in this section can also play a role in producing tensile residual stresses. The work-hardening and defect density gradient beneath the machined surface was evaluated using X-ray peak half-width measurement. The results, obtained on the same specimens as in Figure 3, are depicted in Figure 8 for different cutting speeds and cutting depths. Figure 8(a) illustrates the very steep decrease of the half width in the first 20 to 30 μm beneath the surface which causes greater elastic relaxation of the near-surface layer with respect to the underlying material. Furthermore, it can be seen from Figure 8(a) that increasing the cutting speed leads to decreasing values of the X-ray peak half width at a given depth. This underlines the suggestion that at higher cutting speeds, the (compressive) plastic deformation and the microstructural defect density in the surface layer are decreased.

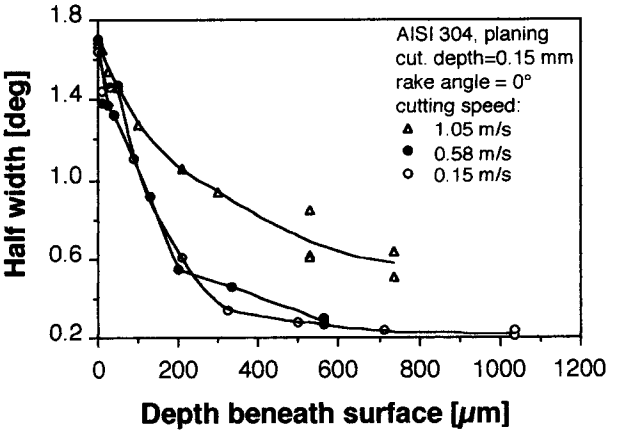

(*a*)

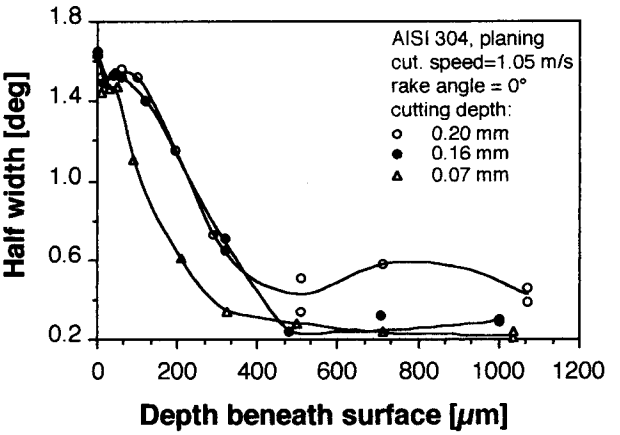

(*b*)

Fig. 8 — Influence of (*a*) cutting speed and (*b*) cutting depth on measured X-ray diffraction peak half-width profiles (an indication of defect density and extent of work hardening).

B. *Effect of Cutting Depth*

Figure 7(b) shows that increasing cutting depth does not lead to important variations in the calculated thermal stresses. This is clear since workpiece temperatures and the heated workpiece depth change only a small amount with increasing cutting depth (T_{max} = 310 °C and 280 °C at cutting depths of 0.08 mm and 0.20 mm, respectively) (Figure 5). The reasons for this can be found in the chip formation process. Greater cutting depths enlarge the shear

angle during planing (Table I). Thus, the mean distance between the shear plane (*i.e.*, the heat source) and the surface of the workpiece increases with cutting depth, and a greater part of the heat is carried away with the chip before it can be conducted into the workpiece (small thermal diffusivity of this material). This effect is partly compensated by a rise in cutting energy when the cutting depth is increased. Therefore, there is only a small diminution of the workpiece temperatures at increasing cutting depths. It is obvious that similar workpiece temperature fields lead to comparable thermal residual stress distributions, which can be seen from Figure 7(b).

A comparison of the calculated (Figure 7(b)) with the experimental (Figure 3(b)) results indicates that the expanding tensile near-surface residual stress region due to increasing cutting depths must be the result of a greater mechanical impact of the tool. As has been presented in the discussion of the influence of the cutting speed, it is suggested that the additional tensile residual stresses caused by the mechanical impact of the tool are due to compressive plastic deformation ahead of the advancing tool and greater elastic relaxation with respect to underlying material layers of the surface layer which was work hardened and whose defect density was markedly increased during machining. It can be seen from Table I that the working angle decreases when the cutting depth is increased. A decreasing working angle is ascribed to a mechanical influence of the tool which enhances the formation of tensile residual stresses.[12,13] Other factors affecting the extent of compressive plastic deformation discussed before[30] do not change markedly with cutting depth. Therefore, the additional tensile residual stresses are caused by an increasing relaxation effect. This is supported by Figure 8(b), from which it is apparent that the X-ray peak half-width measurements on the same specimens as in Figure 3(b) show an augmentation of the surface value and the thickness of the modified layer beneath the machined surface with increasing cutting depth.

V. CONCLUSIONS

The knowledge of the steady-state workpiece temperatures allows one to calculate the thermal residual stresses which are induced during the machining operation. By comparing the calculated results with experimental values, one can separate the two main influences (thermal/mechanical) on the residual stress state. It was shown that not only the thermal impact of the machining operation but also the mechanical influence of the tool produces tensile residual stresses. It is suggested that this is a result of compressive plastic deformation in the surface layer due to the tool pressure during cutting and greater elastic relaxation of a work-hardened and defect-rich surface layer of the machined specimen with respect to the underlying material. Factors of the mechanical impact which increase tensile residual stresses are a low shear and working angle, a small ratio of tangential to normal stress in the primary deformation zone, and a high work-hardening and microstructural defect gradient beneath the machined surface. Decreasing cutting depth and increasing cutting speed reduce the size of the superficial tensile residual stress region for this material and this machining operation.

ACKNOWLEDGMENTS

Financial support by the Swiss National Science Foundation (Project No. 2000-5.256) is gratefully acknowledged. The author would like to thank Professor Bernhard Ilschner for his encouragement of this work and his constant support, the Laboratoire de Métallurgie Physique for the permission to use the 3-MOLST program to calculate workpiece temperatures, and Drs. Hans-Ulrich Künzi, Andrew F.A. Hoadley, and Ashok Ramteke for fruitful discussions.

REFERENCES

1. C. Wiesner, H.-U. Künzi, and B. Ilschner: *Mater. Sci. Eng.*, 1991, vol. A145, pp. 151-58.
2. F. Dupont, C.A. Brown, and B. Ilschner: *Z. Metallkd.*, 1988, vol. 79, pp. 74-80.
3. B. Scholtes: in *Proc. Adv. in Surface Treatment: Technology-Application-Effects Vol. 4 Residual Stress*, Pergamon Press, Oxford, 1987, pp. 59-71.
4. *Eigenspannungen und Lastspannungen*, V. Hauk and E. Macherauch, eds., Carl Hanser Verlag, Munich, 1982.
5. I.C. Noyan and J.B. Cohen: *Residual Stresses*, Springer-Verlag, New York, NY, 1987.
6. *Proc. 28th Sagamore Army Res. Conf.: Residual Stress and Stress Relaxation*, E. Kula and V. Weiss, eds., Plenum Press, New York, NY, 1982.
7. *Residual Stresses: Origin-Evaluation-Calculation-Measurement*, E. Macherauch and V. Hauk, eds., Deutsche Gesellschaft für Materialkunde, Oberursel, 1986.
8. H. Dölle and J.B. Cohen: *Metall. Trans. A*, 1980, vol. 11A, pp. 831-38.
9. C.R. Liu, Z.C. Lin, and M.M. Barash: in *Proc. Conf. High Speed Machining*, ASME, Fairfield, NJ, Report No. PED-vol. 12, pp. 181-91.
10. T. Kagiwada and T. Kanauchi: *Bull. Jpn. Soc. Prec. Eng.*, 1981, vol. 15, pp. 195-96.
11. H. Eda and K. Kishi: *Werkstatt Betr.*, 1986, vol. 119, pp. 1019-24.
12. K. Okushima and Y. Kakimo: *Mem. Faculty Eng. Kyoto Univ. Jpn.*, 1972, vol. 34, pp. 234-48.
13. K. Okushima and Y. Kakimo: *Ann. CIRP*, 1971, vol. 20 (1), pp. 13-14.
14. C. Wiesner, A.F.A. Hoadley, M. Ramaroson, and B. Ilschner: *Mat.-wiss. u. Werkstofftech.*, 1990, vol. 21, pp. 194-206.
15. *Härtereitechnische Mitteilungen*, 1976, vol. 31, issues 1 and 2.
16. C. Wiesner: Ph.D. Thesis, Swiss Institute of Technology, Lausanne, 1991.
17. I.C. Noyan: *Metall. Trans. A*, 1983, vol. 14A, pp. 1907-14.
18. I.C. Noyan and J.B. Cohen: *Adv. X-Ray Anal.*, 1983, vol. 27, pp. 129-48.
19. B. Scholtes and O. Vöhringer: in *Proc. Mechanische Oberflächenbehandlung: Festwalzen-Kugelstrahlen-Sonderverfahren*, Deutsche Gesellschaft für Material kunde, Oberursel, 1989, pp. 3-20.
20. M. Field: *Trans. Am. Soc. Mech. Eng., J. Eng. Ind.*, 1976, vol. 98, pp. 1192-1201.
21. M.M. Barash and L.R. Liu: *Trans. Am. Soc. Mech. Eng., J. Eng. Ind.*, 1982, vol. 104, pp. 257-64.
22. M.M. Barash and L.R. Liu: in *Proc. Inter-American Conf. on Mater. Technol.*, San Francisco, CA, 1980, pp. 171-75.
23. E. Brinksmeier, J.T. Cammet, W. König, P. Leskovar, J. Peters, and H.K. Tönshoff: *Ann. CIRP*, 1982, vol. 31/2, pp. 491-510.
24. M. Rappaz, B. Carrupt, M. Zimmermann, and W. Kurz: *Helv. Phys. Acta*, 1987, vol. 60, pp. 924-36.
25. A.F.A. Hoadley, M. Rappaz, and M. Zimmermann: *Metall. Trans. B*, 1991, vol. 22B, pp. 101-09.

26. ABAQUS Version 4-8-5, Users, Theory and Examples Manuel, Hibbit, Karlsson & Sorensen Inc., Providence, RI, 1989.
27. M.F. Kanninen, F.W. Brust, J. Ahmed, and I.S. Abou-Sayed: in *Proc. 28th Sagamore Army Res. Conf.: Residual Stress and Stress Relaxation*, E. Kula and V. Weiss, eds., Plenum Press, New York, NY, 1982, pp. 227-36.
28. C.A. Brown, F. Dupont, E. El Batawi, and B. Ilschner: *Microstruct. Sci.*, M. Blum, ed., 1987, vol. 15, pp. 383-92.
29. C.R. Liu and Z.C. Lin: *Int. J. Mech. Sci.*, 1985, vol. 27, pp. 281-91.
30. D.W. Wu and Y. Matsumato: *Trans. Am. Soc. Mech. Eng., J. Eng. Ind.*, 1990, vol. 112, pp. 245-52.